ACS APPLIED MATERIALS & INTERFACES

Research Article

www.acsami.org

Exclusively Gas-Phase Passivation of Native Oxide-Free Silicon(100) and Silicon(111) Surfaces

Ye Tao,*[,†,‡] Roland Hauert,[§] and Christian L. Degen[†]

[†]Department of Physics, ETH Zürich, 8093 Zürich, Switzerland

[‡]Department of Chemistry, Massachusetts Institute of Technology, Cambridge, Massachusetts 02139, United States

[§]Empa, Swiss Federal Laboratories of Materials Science and Technology, 8600 Dübendorf, Switzerland

Supporting Information

ABSTRACT: Reactions in the gas phase are of primary technological importance for applications in nano- and microfabrication technology and in the semiconductor industry. We present exclusively gas-phase protocols to chemically passivate oxide-free Si(111) and Si(100) surfaces with short-chain alkynes. The resulting surfaces showed equal or better oxidation resistance than most existing liquid-phase-derived surfaces and rivaled the outstanding stability of a full-coverage Si(111)−propenyl surface.[1,2] The most stable surface (Si(111)−ethenyl) grew one-fifth of a monolayer of oxide (0.04 nm) after 1 month of air exposure. We monitored the regrowth of oxides on passivated Si(111) and Si(100) surfaces by X-ray photoelectron spectroscopy (XPS) and observed a significant crystal-orientation dependence of initial rates when total oxide thickness was below approximately one monolayer (0.2 nm). This difference was correlated with the desorption kinetics of residual surface Si−F bonds formed during HF treatment. We discuss applications of the technology and suggest future directions for process optimization.

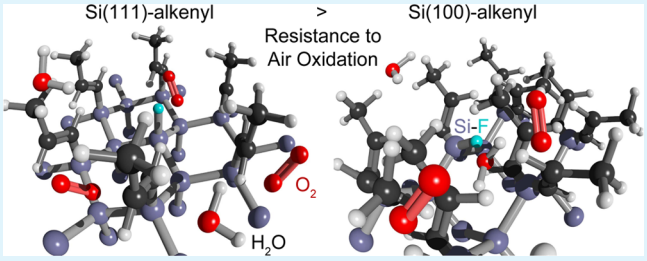

KEYWORDS: *single-crystal silicon, gas-phase processing, surface oxidation mechanism, crystal orientation dependence, gas-phase doping*

INTRODUCTION

The chemical passivation of oxide-free silicon surfaces by Si−C monolayers[1−19] improves both the electrical and the mechanical properties of a variety of silicon-based devices. Si−C monolayers can, for example, enhance the performance of silicon-based photovoltaic devices,[20,21] increase the sensitivity of silicon field-effect sensors and devices,[22−24] act as a dielectric layer with tunable tunneling barrier,[25,26] provide a path to precision surface doping,[27] and reduce electromechanical dissipations in nanoelectromechanical systems (NEMS).[28−30] Due to its often easy integration into wafer-scale processes, the technology provides an important opportunity for industrial applications.

While working to improve the mechanical properties of silicon-based NEMS and MEMS devices,[30] we discovered that the vast majority of Si−C formation reactions rely on liquid-phase chemistry. Liquid-phase processes are incompatible with delicate NEMS that are susceptible to mechanical failure by sonication, agitation, or surface tension and that are extremely sensitive to surface contamination by insoluble residues and metallic impurities.[31−33] This is especially true in the final stages of fabrication.[30,34,35] Besides such structural issues, the liquid-phase fluoride etching step (HF, NH_4F, or buffered HF), necessary for removing the native oxide, also attacks other common structural and functional materials in nanofabricated devices, including dielectric spacers, metallic contacts,[36,37] and even the silicon itself by metal-assisted etching.[38] Finally, existing Si−C surfaces, with the exception of the Si(111)−propenyl surface, suffer from finite air stability with oxide regrowth time constants typically on the order of days to weeks.[1,2,39]

Complications arising from liquid-phase chemistry can be circumvented via gas-phase reactions. Gas-phase HF etching, for instance, can be tuned to drastically improve etching selectivity to avoid and minimize damage to other materials in a device.[40,41] Initial attempts included gas-phase hydrosilylation reactions aiming for high surface coverage[42−44] and mechanistic understanding.[45] These pioneering efforts employed standard liquid-phase fluoride etching for native-oxide removal[42,43] and a specialized in-situ-synthesized H-terminated nanoparticle substrate.[44] On a longer run, gas-phase reactions could provide many additional advantages, including reagent−solvent economy, cleanliness,[46] better etching selectivity resulting in wider material compatibility,[40,41] as well as procedural simplicity. These are expected to facilitate integration into automated,

Received: March 18, 2016
Accepted: May 6, 2016
Published: May 6, 2016

DOI: 10.1021/acsami.6b03326
ACS Appl. Mater. Interfaces 2016, 8, 13157−13165

vacuum-processing sequences that are standard in the semiconductor industry.

With the goal of a generally applicable method in mind, we developed a set of exclusively gas-phase reaction sequences to prepare native oxide-free, C-terminated silicon(100) and silicon(111) surfaces. We found that the resulting surfaces exhibited similar or better air stabilities than liquid-phase-prepared, fully covered alkyl− and alkynyl−Si(111) surfaces. The best protocols led to stabilities approaching that of the fully alkylated Si(111)-propenyl surface.[2] We used X-ray photoelectron spectroscopy (XPS) to study the mechanism of native-oxide regrowth and monolayer aging in air. We found that passivated Si(111) surfaces were significantly more stable than identically treated Si(100) surfaces in the initial stages of oxide regrowth. We discuss possible mechanisms behind the oxidative degradation and suggest future avenues for further optimizing the surface stability.

EXPERIMENTAL SECTION

Details of the processing can be found in the Supporting Information (SI). Briefly, we removed carbonaceous adsorbates from as-purchased wafers by a UV−ozone treatment or an oxygen plasma ashing step. The surface oxide was then removed via gas-phase hydrofluoric acid etching.[40,41] The Si−C bond was finally formed by thermal or photochemical hydrosilylation with gaseous terminal alkynes at a pressure of 1 atm inside a custom-built high-vacuum reaction chamber. After hydrosilylation, samples were put inside waffle-pack boxes, wrapped in aluminum foil, and stored in ambient atmosphere (23 ± 2 °C, 50 ± 10% humidity). We chose octene and propyne as our model reagents as their hydrosilylation products, respectively, represent a prototypical alkyl monolayer and the ultrastable Si−propenyl benchmark surface. We also used acetylene, 3,3,3-trifluoropropyne, cyanoacetylene, and trivinylphosphine to probe the effects of reactant geometry and electronic properties and to test applicability in doping applications.

We note that during the course of this study we used the same 1 atm (in reactor volume) of each alkyne gas for more than 100 reaction runs by recondensing the gases back into their respective reservoirs. We have not noticed a visible decrease in the amount (1−2 mL) of recollected compounds. This observation clearly highlights the reagent economy, cleanliness, and procedural simplicity of gas-phase processes.

RESULTS AND DISCUSSION

Gas-Phase Processing Achieves Excellent Passivation Effect. We first assessed whether gas-phase processing is a potentially useful approach capable of producing films with good air stability. While the most rigorous comparison between liquid- and gas-phase processes should employ products from the same chemical reaction taking place in different phases, hydrosilylation of propyne in liquid has not been reported and important benchmark surfaces like the Si−Me and Si−propynyl can only be prepared using two-step processes. Figure 1A therefore compares the native oxide regrowth kinetics of exclusively gas-phase-processed Si(111) samples with those of comparable Si(111) samples prepared by the standard liquid-phase two-step chlorination−Grignard alkylation sequence.

The data showed that gas-phase H-terminated and octyl-terminated surfaces had comparable stabilities as liquid-phase H-terminated and alkyl-terminated surfaces. Gas-phase propenyl samples showed stabilities that were intermediate between those of solution-phase methyl and propenyl samples. A possible explanation of the difference in stabilities between liquid-phase and gas-phase Si(111)−propenyl surfaces is the presence of residual Si−F bonds on the latter, which can limit the maximum attainable Si−C coverage in subsequent

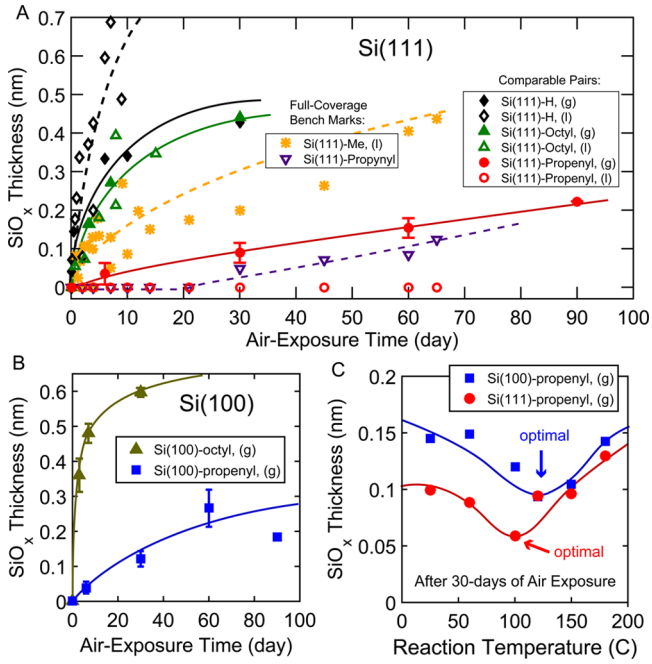

Figure 1. (A) Kinetics of native oxide regrowth on representative gas-phase- and liquid-phase-processed Si(111) samples. Data were taken by X-ray photoelectron spectroscopy (XPS) and plotted in thickness units for intuitive clarity (see SI). Gas-phase data (filled symbols and solid lines) are from this study. Liquid-phase data (open symbols and dashed lines) are literature values.[1,39] Dashed line for liquid-phase octyl samples is omitted. Error bars for gas-phase data are standard errors from multiple experimental runs, some at different temperatures. (B) Kinetics of native oxide regrowth on gas-phase-processed Si(100) samples. (C) Thickness of regrown oxide on identically treated pairs of Si(111) and Si(100) plotted as a function of hydrosilylation temperature. Solid and dashed lines are guides to the eye.

hydrosilylation. This and additional points will be discussed in detail.

Figure 1B plots analogous oxide regrowth data for Si(100) surfaces with a qualitatively similar result to that of Si(111).

Figure 1C further shows that the optimal reaction temperature for propyne hydrosilylation was between 100 and 120 °C. The existence of an optimal temperature can be expected: monolayer formation on a surface requires adsorption as a first step, which would become unfavorable at high temperatures due to entropic penalty. Similar results for acetylene are provided in the SI. The data also suggested that Si(111) surfaces are slightly more stable than identically treated Si(100) samples. Even though HF-etched Si(100) and Si(111) surfaces are both microscopically rough, there exist significant differences in the type and percentages of crystalline facets and hydride types (dihydrides-to-monohydrides ratio).[47] We will provide a fuller discussion of this observation later while discussing the mechanism of surface oxidative degradation.

Surfaces Undergo Oxidative Degradation. In order to better understand the air-aging mechanism, we monitored the evolution of the surface atomic composition by XPS for up to 90 days. The chemisorbed and physisorbed molecular population on the surface was found to contain carbon, oxygen, silicon, and fluorine but no other elements (SI). We first focus our attention on the atomic fractions of the majority elements: carbon, oxygen, and silicon (Figure 2). Fluorine was also monitored and is discussed separately in Figure 4.

DOI: 10.1021/acsami.6b03326
ACS Appl. Mater. Interfaces 2016, 8, 13157−13165

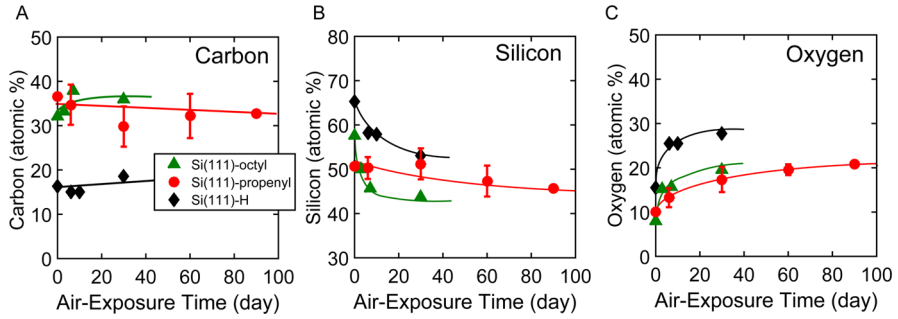

Figure 2. Changes in the atomic percentage of surface carbon (A), silicon (B), and oxygen (total oxygen including SiO_x and in all other forms) (C) as samples were exposed to air for up to 3 months. Data are for Si(111) samples. Si(100) samples showed similar trends (SI). Solid lines are guides to the eye.

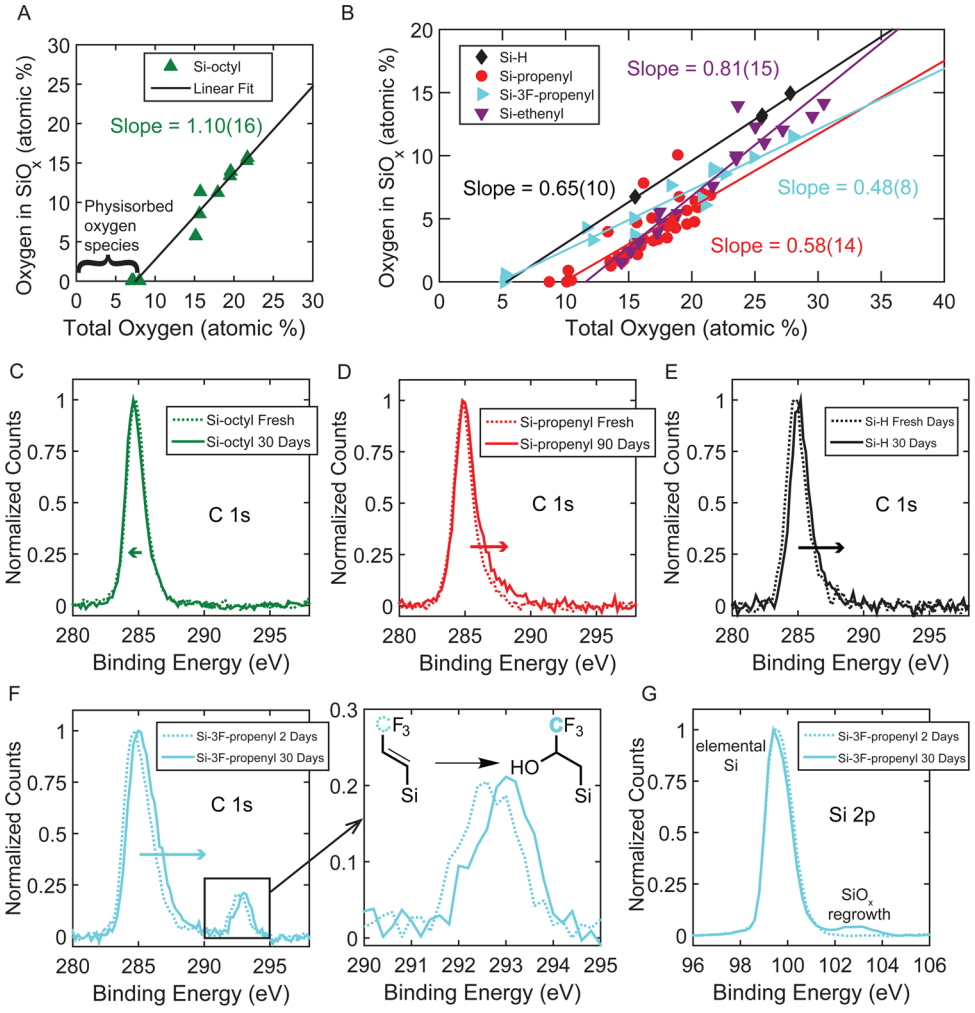

Figure 3. Different surface organic coatings exhibit different affinities for oxygen. (A) Amount of oxygen atoms in the form of SiO_x as a function of the total amount of oxygen on Si−octyl surfaces. (B) Equivalent data for Si−H, Si−propenyl, Si−3,3,3-trifluoropropenyl, and Si−ethenyl surfaces. (C−F) Air aging-induced carbon 1s spectral change for Si−octyl, Si−propenyl, Si−H, and Si−3,3,3-trifluoropropenyl surfaces. Arrows indicate the direction and magnitude of the observed spectral shift. (G) Silicon 2p peaks corresponding to samples in F. Data in A and B are combined Si(111) and Si(100) data sets. For clarity, only one crystal orientation is shown in C−F. Data for both crystal orientations are consistent (SI). Solid lines are linear fits to the data.

The atomic concentration values were obtained by dividing the peak areas by the respective sensitivity factors and normalizing against the sum. We did not, however, adopt a particular structural model of the surface in preparing Figure 2. This was because of two reasons: (a) Data as presented in Figure 2 is for an initial, qualitative assessment to obtain a rough picture of the chemical evolution of the surfaces upon air aging. (b) Qualitative trends in the relative changes of different elements is necessary for justifying an explicit structural model needed for subsequent quantitative analyses.

Figure 2A shows that the hydrogen-terminated surface had about 15 atom % of carbon. This value represents a typical level

DOI: 10.1021/acsami.6b03326
ACS Appl. Mater. Interfaces 2016, 8, 13157−13165

of adventitious organic carbon physisorption.[48] The ratios of C 1s peak area to Si 2p peak area on these samples are between 0.19 and 0.27, agreeing quantitatively with literature data.[48] Exposures to gaseous octene and propyne increased the surface density of carbon-containing species above the background physisorption level. The magnitude of the increase is consistent with the addition of roughly another monolayer of carbonaceous adsorbate, most likely covalently bound for reasons including the following. Sonication cleaning of a functionalized Si(111)−ethenyl sample in methanol and dichloromethane for 5 min each only reduced the carbon to 29 atom %. Physisorbed monolayers do not offer oxidation resistance (as on Si−H), or the two curves in Figure 1B would have been interchanged due to the relative volatilities of octene and propyne.

Figure 2B and 2C, respectively, plots the evolution of silicon and oxygen concentrations. While the silicon concentration decreased, the oxygen concentration increased and the sum of Si and O contributions was roughly constant with time. This observation suggests that oxygen-containing species were added above the silicon crystal. The oxygen concentration can increase in two ways. A first pathway is native oxide regrowth when O_2 and H_2O molecules chemically react with the underlying silicon lattice. Alternatively, oxygen-containing molecules may accumulate via physisorption and/or chemical reaction with the organic monolayer.

Oxygen-Containing Species Interact with the Organic Overlayer. To identify the dominant pathway for oxygen accretion, we divided the oxygen population into forms of silicon oxides (SiO_x) and in all other forms.

This distinction was possible because the amount and type of silicon oxides can be determined by analyzing the Si 2p region of the XPS spectra (SI). Figure 3A plots the atomic percentage of silicon-bound oxygen versus that of all oxygen species on the octyl samples. The axes are on the same scale as both percentages are referenced to the total surface atomic population (all elements) probed by the spectrometer. The plot indicates that additional oxygen beyond a threshold concentration of about 7% was added in the form of SiO_x (straight line fit with slope 1.10 ± 0.16). Oxygen therefore added to the Si−octyl surfaces predominantly via silicon native oxide regrowth.

Figure 3B plots the corresponding data for Si−H (slope 0.65 ± 0.10), Si−propenyl (0.58 ± 0.14), Si−ethenyl (0.81 ± 0.15), and Si−3,3,3-trifluoropropenyl (0.48 ± 0.08) samples. The last two types of surfaces were fabricated to probe the mechanism of film aging. The data are qualitatively similar to those for octyl surfaces, but slope values are significantly less than unity. This suggests that for these films additional oxygen present on the surface was only partially incorporated in the form of native oxide.

We believe that the significant differences between surfaces are due to both physisorption and chemical reactions, depending on the surfaces under study. For example, between Si−octyl and Si−H, the different oxygen incorporation may be due to differences in incremental water adsorption and possibly a changing composition in the physisorption layer. In octyl samples, the growing hydrophilic oxide is buried underneath a hydrophobic monolayer. On bare Si−H surfaces, the growing oxide layer is directly exposed to the atmosphere. Therefore, physical processes alone would be sufficient to account for the observations.

Differences between the Si−octyl and the Si−alkenyl samples, in contrast, may entail an additional chemical component. It is tempting to invoke an oxidation process of the covalently attached, unsaturated organic moiety; after all, Si−alkenyl surface groups are vinylsilanes that are capable of undergoing oxygen addition reactions such as dihydroxylation.[49] Such chemical transformations would increase the hydrophilicity of the covalent monolayer, which could in turn lead to a dynamic increase of the oxygen content of the physisorption layer.

Time evolution in the C 1s XPS spectra provides conclusive experimental evidence for chemical changes in the carbon overlayer. We observed significant spectral shifts to higher binding energies in the Si−H, Si−propenyl, and 3,3,3-trifluoropropenyl samples with time (Figure 3D−F and SI). The direction of these shifts is consistent with increases of the average oxidation state of carbon. We verified that shifts in carbon peaks are not due to a global shift of the spectra, as the position of the elemental Si is unchanged for the as-prepared and the air-exposed samples (Figure 3G). In contrast, hardly any change was visible in the octyl samples (Figure 3C). In particular, the significant chemical shift of the well-revolved $-CF_3$ peak on trifluoromethylpropenyl surfaces can only occur following oxidation of the neighboring carbon atoms (Figure 3F). The data are therefore consistent with a scenario where oxygen-rich species interacted chemically with the unsaturated, covalently bound organic monolayers as well as physically with an exposed native oxide surface.

Alternative explanations for the observed shifts in C 1s emissions include band bending effects and changes in surface dipole or charge accumulation patterns over time. These possibilities are unlikely for reasons including the following. Band bending requires the parallel shift of the Si 2p emissions (Figure 3G) that were not observed. For surface dipole to explain the 0.34 eV shift as in Figure 3F would necessitate a chemical transformation as dramatic as from 100%-coverage Si−Br bond to 100%-coverage $Si-CH_3$.[50] As a result, chemical oxidation of the unsaturated surface alkenyl moieties and the resulting chemical shift by induction appears to be the most likely explanation.

To the best of our knowledge, there is no analytical technique currently available that is capable of conclusively verifying the mechanism behind the observed chemical transformation. We therefore take a naïve approach to speculate on two plausible pathways for the oxidation of surface alkenyl carbon chains. While we describe each as a stepwise mechanism for narrative clarity, we note that their concerted analogues may also be operative. We also note that due to the very slow experimentally observed oxygen incorporation rates, low-probability elementary steps cannot be ignored and may be invoked.

A first possible scenario is based on the well-known charge-transfer doping mechanism at the surface of semiconductor materials including diamond, silicon, and carbon nanotubes.[51−60] Physisorbed monolayers of organic and inorganic molecules or thin films can either donate conduction electrons to the bulk substrate or absorb electrons from the substrate. A chemisorbed organic monolayer can conceivably loose/gain electrons to/from the substrate by the same charge-transfer doping mechanism. If a chemisorbed propenyl group lost an electron to the bulk silicon, possibly via recombination with a hole found in the boron-doped substrate material, a radical cation (radical on α-carbon and charge on the β-carbon) stabilized by hyperconjugation with the Si−C bond (i.e., the β-silicon effect[61]) would form. Physisorbed molecular oxygen or

DOI: 10.1021/acsami.6b03326
ACS Appl. Mater. Interfaces 2016, 8, 13157−13165

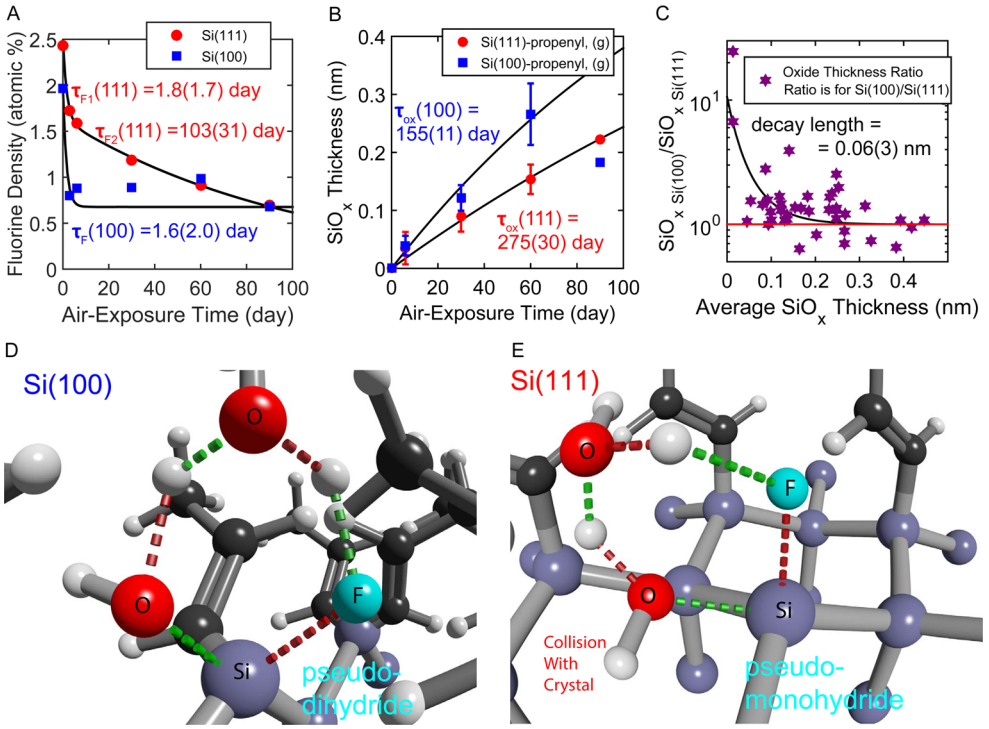

Figure 4. Si(100) surfaces show faster fluorine desorption and oxide growth than Si(111). (A) Surface fluorine concentration as a function of air exposure. Desorption from Si(100) occurs in a single, fast step with an exponential decay constant of 1.6 ± 2.0 days. Desorption from Si(111) shows a fast (rate constant 1.8 ± 1.7 days) and a slow component (rate constant 103 ± 31 days). Solid lines are mono- and biexponential fits. Data are from Si−propenyl and Si−octyl samples. (B) Corresponding regrowth of oxide. Solid lines are monoexponential fits that assume a final native oxide thickness of 0.8 nm (see main text for discussion). The fitted exponential rate constants were 155 ± 11 days for the Si(100) data set and 275 ± 30 days for the Si(111) data set. (C) Pair-wise ratio of oxide thicknesses for identically treated Si(100) and Si(111) surfaces. Data are from 40 Si(100)−Si(111) pairs and plotted as a function of the average thickness of the two samples in each pair. (D and E) Schematic illustrations of the transition states for Si−F hydrolysis by a pair of water molecules on Si(100)−propenyl and Si(111)−propenyl surfaces, respectively. Green dotted lines are incipient bonds, and red dotted lines are breaking bonds.

hydrated ions are alternative electron acceptors that could promote the formation of a radical cation without invoking the charge-transfer doping mechanism.[51,53,62] The carbocation would then be susceptible to nucleophilic attack by oxygen-centered nucleophiles like water. Within the context of this mechanism, the higher slope value of the Si−ethenyl samples compared to that of the Si−propenyl samples may be due to the reduced stability of the primary carbocation intermediate (Figure 3B).

A second possible mechanism based on the α-silicon effect[63] involves the direct nucleophilic attack by an oxygen-centered nucleophile on the β-carbon, with the resulting excess negative charge on the α-carbon stabilized by the neighboring silicon atom. A proton-shuffling step mediated by other water molecules (invariably found in the vicinity under ambient storage conditions) or by other types of hydroxyl groups would subsequently quench the negative charge. Since the trifluoromethyl group inductively increases the electrophilicity of the β-carbon, the lower slope value of the trifluoropropenyl surfaces would be consistent with this pathway (Figure 3B).

Fluorine Atoms Show Crystal Orientation-Dependent Lability. The XPS analysis also revealed a low concentration of residual fluorine on all surfaces. The chemical shift of the fluorine peak was 686.4(2) eV, indicating covalently bonded Si−F that was a remnant from the oxide removal step by hydrofluoric acid vapor.[48,64] The evolution of the fluorine atom surface concentration was highly interesting, as it displayed a significant difference between (100) and (111) crystal orientations. Figure 4A shows that the surface had an initial fluorine content of 2−3% that decreased to below 1% during the 3-months aging period. The two data sets in Figure 4A are averaged over samples where time-dependent data were available.

The decrease in fluorine atomic % was faster for (100) surfaces compared to (111) surfaces. The Si(100) data showed a monoexponential decay where the fast-desorbing portion accounted for roughly two-thirds of the fluorine population. By contrast, the Si(111) showed a biexponential decay with a similar fast-desorbing portion but an additional slow-desorbing portion. Here, the fast-desorbing component accounted for roughly one-third of the total population. We further performed a pairwise Wilcoxon signed-rank test on a data set of 74 samples (SI). This statistical test confirmed that the crystal-orientation difference was significant with a Z value of 3.52 ($p < 0.0005$).

Interestingly, the ratios of labile-to-stable fluorine types coincided with the ratios of dihydrides-to-monohydrides on HF-etched Si(111) and Si(100) surfaces.[47] Si(100) is predominantly dihydride-terminated, whereas Si(111) is predominantly monohydrideterminated. If residual Si−F had no positional preference during formation, its distribution in microenvironments, either in a pseudodihydride (Si_2SiHF) or in a pseudomonohydride (Si_3SiF), would reflect the natural abundances of dihydrides and monohydrides. We have performed high-resolution atomic force microscope analyses of various HF-etched surfaces to confirm that our samples

DOI: 10.1021/acsami.6b03326
ACS Appl. Mater. Interfaces 2016, 8, 13157−13165

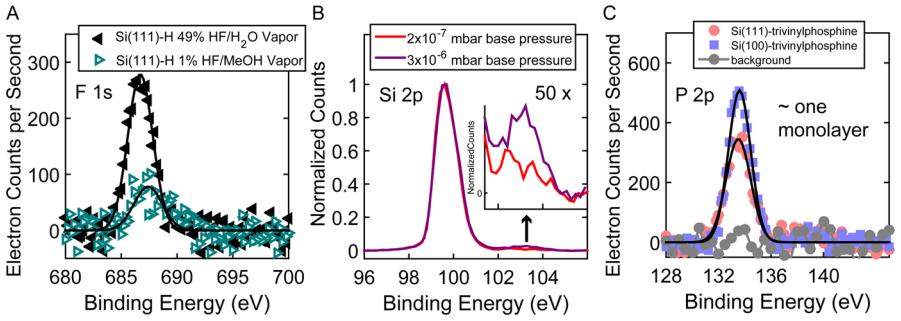

Figure 5. Gas-phase processing could be optimized and extended in several directions. (A) Surface concentration of Si−F is tunable and can be reduced by changing HF vapor composition during initial oxide removal. (B) Better vacuum quality can improve the effectiveness of protection. Si(111)−ethynyl samples prepared at a better base pressure showed less regrown oxides after 1 month of air exposure. (C) Demonstration of phosphorus surface doping in the gas phase using trivinylphosphine. The chemical shift of the phosphine corresponds to a phosphine oxide.

exhibited RMS roughness levels between 0.2 and 0.4 nm that is consistent with this microstructure picture (SI).

The most likely candidate process behind the fluorine decrease is the chemical hydrolysis of Si−F polar bonds. This process has been studied theoretically and experimentally for small organosilanes[65,66] and for the Si(111) surface.[67] We see two prominent reasons why hydrolysis of Si−F on Si(100) should be more efficient than on Si(111).

First, DFT calculations on small model compounds showed that the energetically most favorable transition-state structure is a 6-membered ring involving 2 water molecules.[65] We schematically illustrate this transition state in the context of a surface Si−F bond in Figure 4D and 4E. One of the water molecules plays the role of a dual-activation catalyst: It increases the nucleophilicity of the other water molecule and facilitates the leaving of the fluoride. This occurs in a concerted, proton-shuffling step. For Si−F in a pseudodihydride microenvironment (Figure 4D), the catalytic 6-membered transition state can easily form. The scissile bond is oriented at an angle from the surface normal, leaving room for both the nucleophilic and the catalytic water molecules to approach along the surface normal. In contrast, the catalytic 6-membered transition state cannot easily form within the pseudomonohydride microenvironment predominant on the Si(111) surface (Figure 4E), because it would entail the collision between the nucleophilic water molecule (specifically its spectator proton and lone pair) and the silicon crystal plane. As a result, a catalyzed pathway is not accessible to the pseudomonohydride Si−F.

Second, steric hindrance around the silicon center was found to often determine the kinetics of Si−F hydrolysis.[66] The pseudomonohydride Si−F center is obviously more sterically hindered by the three bulky silyl substituents. In addition, three rigid back bonds limit the freedom of the silicon atom for structural rearrangement when going to the pentavalent transition state. By contrast, strain can relax more efficiently in the case of a pseudodihydride Si−F with only two bonds constrained by the crystal. Therefore, the kinetics of fluorine desorption is consistent with the partitioning into monohydride and dihydride microenvironments on HF-etched Si(111) and Si(100).

The hydrolysis of Si−F may act as the starting point for surface reoxidation. The formation of Si−OH is the initial and rate-limiting step in suboxide formation on Si−H surfaces.[68,69] This step is followed by insertion of oxygen atoms into the adjacent Si−Si back bonds. Figure 4B and 4C indeed confirms that the formation of the first monolayer of oxides proceeds faster on Si(100) samples. Figure 4C plots the ratio of oxide thicknesses on identically treated Si(100) and Si(111) samples as a function of the average oxide thickness of the two samples. Samples are of all types produced in this study. If crystal orientation did not have any bearing on the rate of oxidation, one should obtain points scattered evenly around 1. This is clearly not the case. Figure 4C thus provides conclusive verification of generality (Z score of 3.88, $p < 0.00005$) for the crystal-orientation dependence observed in the propenyl samples (Figure 4B). The dependence fades with a decay length of 0.06(3) nm, indicating that rates mainly differ in the formation of the initial monolayer while subsequent oxide growth is similar. Returning to Figure 3B, we note that propenyl samples showed an increase of up to 7 atom % in SiO_x oxygen, roughly 4 times the fluorine loss. This number makes chemical sense since hydrolytic substitution followed by 3 additional insertions into surrounding back bonds predicts incorporation of roughly 4 oxygen atoms for each leaving fluorine atom.

Future Optimization Strategies and Applications. During the course of this study, a few avenues for future optimization of the gas-phase processing became apparent that are briefly discussed in the following. The most important parameters for improvement appear to be the saturation coverage and pristine monolayer growth conditions with no residual fluorine or oxygen present.

First, we found that the amount of residual fluorine following native oxide removal seems tunable. This is important given that the residual fluorine appears to play an important role in oxide formation. In a test run, we subjected UV−ozone-cleaned samples to a vapor of 1% HF in methanol inside an enclosed vial. Si−H surfaces thus obtained showed more than 50% reduction in residual Si−F concentration (Figure 5A). A more detailed investigation using samples with variable residual Si−F concentrations will be the subject of a future study.

Second, vacuum quality during monolayer formation was found to be important. While all reactions are conducted at 1 atm alkyne pressure, the base pressure before gas introduction is an indication of the cleanliness of the chamber and of its residual oxygen and moisture content. Samples prepared with an elevated base pressure of 3×10^{-6} mbar showed more than twice the amount of oxide regrowth after 1 month (0.04 vs 0.11 nm) as compared to samples prepared at a lower base pressure of 2×10^{-7} (Figure 5B). Even lower pressures could be easily achieved using a load-locked system.

Third, while we employed thermal activation in this study, photochemical assistance might help improve saturation coverage. UV illumination in the gas phase was found to

DOI: 10.1021/acsami.6b03326
ACS Appl. Mater. Interfaces 2016, 8, 13157−13165

promote film growth by polymerization and protection of the underlying silicon against air oxidation (see SI for further discussion).

We finally explored the potential of our gas-phase processes for surface doping of silicon, which is an important technological capability.[27,70] For this purpose we exposed Si–H samples to trivinylphosphine at a vapor pressure of a few percent of an atmosphere. XPS analysis revealed that 4 atom % of phosphorus was attached to the surface, corresponding to about one-quarter of a silicon monolayer and roughly one monolayer of the dopant precursor molecule (Figure 5C). The binding energy of the phosphorus was consistent with that of phosphine oxides,[70] as expected for a sample that was exposed to air for several hours before the measurement. We envision that for future applications, alkynyl phosphines[71] in mixtures with acetylene or propyne could impart concentration tunability and air stability.

CONCLUSION

In conclusion, we demonstrated that stable oxide-free Si(111) and Si(100) surfaces can be produced using exclusive gas-phase processing. The demonstrated air stability is comparable to that achieved by solution-phase methods. Significant mechanistic understanding of native oxide regrowth and organic monolayer degradation has been obtained to guide further optimization of the process. We expect that the presented procedures can be extended with only minor modifications to other important materials, including germanium,[72] silicon carbide,[73] and diamond.[74] The procedural simplicity, cleanliness, gentleness, reagent economy, and full compatibility with standard clean-room technology of gas-phase processes are advantages that we believe will be of great benefit to silicon NEMS in research and industry.

ASSOCIATED CONTENT

Supporting Information

The Supporting Information is available free of charge on the ACS Publications website at DOI: 10.1021/acsami.6b03326.

Experimental setup and procedures, complete XPS characterization data for new surfaces, water contact angle measurements for some surfaces (including Si–oxide, Si–H, Si–ethenyl), details of C 1s peak shift quantification presented in Figure 3G, temperature dependence of the acetylene reaction, and pertinent discussions (PDF)

AUTHOR INFORMATION

Corresponding Author

*E-mail: ytao@phys.ethz.ch,yetao@mit.edu. Phone: +41 (0)44 633 22 20. Fax: +41 (0)44 633 10 56.

Notes

The authors declare no competing financial interest.

ACKNOWLEDGMENTS

The authors thank Professor Louis Cuccia at Concordia University for helpful comments and Dr. Zonglin Chu at the University of Zurich for assistance with water contact angle measurements discussed in the Supporting Information. We thank Christoph Keck for assistance with maintaining the reaction setup in good working order. This work has been supported by the ERC through starting grant 309301 and through NCCR QSIT.

REFERENCES

(1) Puniredd, S. R.; Assad, O.; Haick, H. Highly Stable Organic Monolayers for Reacting Silicon with Further Functionalities: The Effect of the C-C Bond Nearest the Silicon Surface. *J. Am. Chem. Soc.* **2008**, *130*, 13727–13734.

(2) Puniredd, S. R.; Assad, O.; Haick, H. Highly Stable Organic Modification of Si(111) Surfaces: Towards Reacting Si with Further Functionalities while Preserving the Desirable Chemical Properties of Full Si-C Atop Site Terminations. *J. Am. Chem. Soc.* **2008**, *130*, 9184–9185.

(3) Linford, M. R.; Chidsey, C. E. D. Alkyl Monolayers Covalently Bonded to Silicon Surfaces. *J. Am. Chem. Soc.* **1993**, *115*, 12631–12632.

(4) Linford, M. R.; Fenter, P.; Eisenberger, P. M.; Chidsey, C. E. D. Alkyl Monolayers on Silicon Prepared from 1-Alkenes and Hydrogen-Terminated Silicon. *J. Am. Chem. Soc.* **1995**, *117*, 3145–3155.

(5) de Villeneuve, C. H.; Pinson, J.; Bernard, M. C.; Allongue, P. Electrochemical Formation of Close-Packed Phenyl Layers on Si(111). *J. Phys. Chem. B* **1997**, *101*, 2415–2420.

(6) Bansal, A.; Li, X.; Lauermann, I.; Lewis, N. S.; Yi, S. I.; Weinberg, W. H. Alkylation of Si Surfaces using a Two-Step Halogenation Grignard Route. *J. Am. Chem. Soc.* **1996**, *118*, 7225–7226.

(7) Gurtner, C.; Wun, A. W.; Sailor, M. J. Surface Modification of Porous Silicon by Electrochemical Reduction of Organo Halides. *Angew. Chem., Int. Ed.* **1999**, *38*, 1966–1968.

(8) Robins, E. G.; Stewart, M. P.; Buriak, J. M. Anodic and Cathodic Electrografting of Alkynes on Porous Silicon. *Chem. Commun.* **1999**, 2479–2480.

(9) Cicero, R. L.; Linford, M. R.; Chidsey, C. E. D. Photoreactivity of Unsaturated Compounds with Hydrogen-Terminated Silicon(111). *Langmuir* **2000**, *16*, 5688–5695.

(10) Stewart, M. P.; Buriak, J. M. Exciton-Mediated Hydrosilylation on Photoluminescent Nanocrystalline Silicon. *J. Am. Chem. Soc.* **2001**, *123*, 7821–7830.

(11) Stewart, M. P.; Maya, F.; Kosynkin, D. V.; Dirk, S. M.; Stapleton, J. J.; McGuiness, C. L.; Allara, D. L.; Tour, J. M. Direct Covalent Grafting of Conjugated Molecules onto Si, GaAs, and Pd Surfaces from Aryldiazonium Salts. *J. Am. Chem. Soc.* **2004**, *126*, 370–378.

(12) Sun, Q.-Y.; de Smet, L. C. P. M.; van Lagen, B.; Wright, A.; Zuilhof, H.; Sudhölter, E. J. R. Covalently Attached Monolayers on Hydrogen-Terminated Si(100): Extremely Mild Attachment by Visible Light. *Angew. Chem., Int. Ed.* **2004**, *43*, 1352–1355.

(13) Liu, Y.; Yamazaki, S.; Yamabe, S.; Nakato, Y. A Mild and Efficient Si (111) Surface Modification via Hydrosilylation of Activated Alkynes. *J. Mater. Chem.* **2005**, *15*, 4906–4913.

(14) Bashouti, M. Y.; Stelzner, T.; Berger, A.; Christiansen, S.; Haick, H. Chemical Passivation of Silicon Nanowires with C1-C6 Alkyl Chains through Covalent Si-C Bonds. *J. Phys. Chem. C* **2008**, *112*, 19168–19172.

(15) Scheres, L.; Giesbers, M.; Zuilhof, H. Organic Monolayers onto Oxide-Free Silicon with Improved Surface Coverage: Alkynes versus Alkenes. *Langmuir* **2010**, *26*, 4790–4795.

(16) Zhong, Y. L.; Bernasek, S. L. Mild and Efficient Functionalization of Hydrogen-Terminated Si(111) via Sonochemical Activated Hydrosilylation. *J. Am. Chem. Soc.* **2011**, *133*, 8118–8121.

(17) Huck, L. A.; Buriak, J. M. UV-Initiated Hydrosilylation on Hydrogen-Terminated Silicon (111): Rate Coefficient Increase of Two Orders of Magnitude in the Presence of Aromatic Electron Acceptors. *Langmuir* **2012**, *28*, 16285–16293.

(18) Rijksen, B.; Pujari, S. P.; Scheres, L.; van Rijn, C. J. M.; Baio, J. E.; Weidner, T.; Zuilhof, H. Hexadecadienyl Monolayers on Hydrogen-Terminated Si(111): Faster Monolayer Formation and Improved Surface Coverage Using the Enyne Moiety. *Langmuir* **2012**, *28*, 6577–6588.

(19) Bhairamadgi, N. S.; Pujari, S. P.; Trovela, F. G.; Debrassi, A.; Khamis, A. A.; Alonso, J. M.; Ai Zahrani, A. A.; Wennekes, T.; Al-Turaif, H. A.; van Rijn, C.; Alhamed, Y. A.; Zuilhof, H. Hydrolytic and

DOI: 10.1021/acsami.6b03326
ACS Appl. Mater. Interfaces 2016, 8, 13157–13165

Thermal Stability of Organic Monolayers on Various Inorganic Substrates. *Langmuir* **2014**, *30*, 5829−5839.
(20) Shen, X.; Sun, B.; Yan, F.; Zhao, J.; Zhang, F.; Wang, S.; Zhu, X.; Lee, S. High-Performance Photoelectrochemical Cells from Ionic Liquid Electrolyte in Methyl-Terminated Silicon Nanowire Arrays. *ACS Nano* **2010**, *4*, 5869−5876.
(21) Shen, X.; Sun, B.; Liu, D.; Lee, S.-T. Hybrid Heterojunction Solar Cell Based on Organic-Inorganic Silicon Nanowire Array Architecture. *J. Am. Chem. Soc.* **2011**, *133*, 19408−19415.
(22) Bunimovich, Y. L.; Shin, Y. S.; Yeo, W.-S.; Amori, M.; Kwong, G.; Heath, J. R. Quantitative Real-Time Measurements of DNA Hybridization with Alkylated Nonoxidized Silicon Nanowires in Electrolyte Solution. *J. Am. Chem. Soc.* **2006**, *128*, 16323−16331.
(23) He, T.; He, J.; Lu, M.; Chen, B.; Pang, H.; Reus, W. F.; Nolte, W. M.; Nackashi, D. P.; Franzon, P. D.; Tour, J. M. Controlled Modulation of Conductance in Silicon Devices by Molecular Monolayers. *J. Am. Chem. Soc.* **2006**, *128*, 14537−14541.
(24) Bashouti, M. Y.; Tung, R. T.; Haick, H. Tuning the Electrical Properties of Si Nanowire Field-Effect Transistors by Molecular Engineering. *Small* **2009**, *5*, 2761−2769.
(25) Liu, Y.-J.; Yu, H.-Z. Alkyl Monolayer-Passivated Metal-Semiconductor Diodes: Molecular Tunability and Electron Transport. *ChemPhysChem* **2002**, *3*, 799−802.
(26) Salomon, A.; Boecking, T.; Chan, C. K.; Amy, F.; Girshevitz, O.; Cahen, D.; Kahn, A. How Do Electronic Carriers Cross Si-Bound Alkyl Monolayers? *Phys. Rev. Lett.* **2005**, *95*, 266807.
(27) Ho, J. C.; Yerushalmi, R.; Jacobson, Z. A.; Fan, Z.; Alley, R. L.; Javey, A. Controlled Nanoscale Doping of Semiconductors via Molecular Monolayers. *Nat. Mater.* **2008**, *7*, 62−67.
(28) Haick, H.; Hurley, P. T.; Hochbaum, A. I.; Yang, P.; Lewis, N. S. Electrical Characteristics and Chemical Stability of Non-Oxidized, Methyl-Terminated Silicon Nanowires. *J. Am. Chem. Soc.* **2006**, *128*, 8990−8991.
(29) Henry, J. A.; Wang, Y.; Hines, M. A. Controlling Energy Dissipation and Stability of Micromechanical Silicon Resonators with Self-assembled Monolayers. *Appl. Phys. Lett.* **2004**, *84*, 1765−1767.
(30) Tao, Y.; Navaretti, P.; Hauert, R.; Grob, U.; Poggio, M.; Degen, C. L. Permanent Reduction of Dissipation in Nanomechanical Si Resonators by Chemical Surface Protection. *Nanotechnology* **2015**, *26*, 465501.
(31) Tas, N.; Sonnenberg, T.; Jansen, H.; Legtenberg, R.; Elwenspoek, M. Stiction in Surface Micromachining. *J. Micromech. Microeng.* **1996**, *6*, 385−397.
(32) van Spengen, W. M. MEMS Reliability from a Failure Mechanisms Perspective. *Microelectron. Reliab.* **2003**, *43*, 1049−1060.
(33) Lupina, G.; Kitzmann, J.; Costina, I.; Lukosius, M.; Wenger, C.; Wolff, A.; Vaziri, S.; Ostling, M.; Pasternak, I.; Krajewska, A.; Strupinski, W.; Kataria, S.; Gahoi, A.; Lemme, M. C.; Ruhl, G.; Zoth, G.; Luxenhofer, O.; Mehr, W. Residual Metallic Contamination of Transferred Chemical Vapor Deposited Graphene. *ACS Nano* **2015**, *9*, 4776−4785.
(34) Yang, J. L.; Ono, T.; Esashi, M. Energy Dissipation in Submicrometer Thick Single-Crystal Silicon Cantilevers. *J. Microelectromech. Syst.* **2002**, *11*, 775−783.
(35) Tao, Y.; Boss, J. M.; Moores, B. A.; Degen, C. L. Single-Crystal Diamond Nanomechanical Resonators with Quality Factors Exceeding One Million. *Nat. Commun.* **2014**, *5*, 3638.
(36) Williams, K. R.; Muller, R. S. Etch Rates for Micromachining Processing. *J. Microelectromech. Syst.* **1996**, *5*, 256−269.
(37) Williams, K. R.; Gupta, K.; Wasilik, M. Etch Rates for Micromachining Processing-Part II. *J. Microelectromech. Syst.* **2003**, *12*, 761−778.
(38) Peng, K. Q.; Yan, Y. J.; Gao, S. P.; Zhu, J. Synthesis of Large-Area Silicon Nanowire Arrays via Self-Assembling Nanoelectrochemistry. *Adv. Mater.* **2002**, *14*, 1164−1167.
(39) Webb, L. J.; Lewis, N. S. Comparison of the Electrical Properties and Chemical Stability of Crystalline Silicon(111)Surfaces Alkylated Using Grignard Reagents or Olefins with Lewis Acid Catalysts. *J. Phys. Chem. B* **2003**, *107*, 5404−5412.
(40) Watanabe, H.; Ohnishi, S.; Honma, I.; Kitajima, H.; Ono, H.; Wilhelm, R. J.; Sophie, A. J. L. Selective Etching of Phosphosilicate Glass with Low Pressure Vapor HF. *J. Electrochem. Soc.* **1995**, *142*, 237−243.
(41) Witvrouw, A.; Du Bois, B.; Verbist, A.; Van Hoof, C. A.; Bender, H.; Baert, C. Comparison Between Wet HF Etching and Vapor HF Etching for Sacrificial Oxide Removal. *Proc. SPIE* **2000**, *130*, 130.
(42) Kosuri, M. R.; Gerung, H.; Li, Q.; Han, S. M.; Bunker, B. C.; Mayer, T. M. Vapor-Phase Adsorption Kinetics of 1-Decene on H-Terminated Si(100). *Langmuir* **2003**, *19*, 9315−9320.
(43) Kosuri, M. R.; Gerung, H.; Li, Q.; Han, S. M.; Herrera-Morales, P. E.; Weaver, J. F. Vapor-Phase Adsorption Kinetics of 1-decene on Hydrogenated Si(111). *Surf. Sci.* **2005**, *596*, 21−38.
(44) Jariwala, B. N.; Dewey, O. S.; Stradins, P.; Ciobanu, C. V.; Agarwal, S. In Situ Gas-Phase Hydrosilylation of Plasma-Synthesized Silicon Nanocrystals. *ACS Appl. Mater. Interfaces* **2011**, *3*, 3033−3041.
(45) Eves, B. J.; Lopinski, G. P. Formation of Organic Monolayers on Silicon via Gas-Phase Photochemical Reactions. *Langmuir* **2006**, *22*, 3180−3185.
(46) Lee, Y.-I.; Park, K.-H.; Lee, J.; Lee, C.-S.; Yoo, H. J.; Kim, C.-J. C.; Yoon, Y.-S. Dry Release for Surface Micromachining with HF Vapor-Phase Etching. *J. Microelectromech. Syst.* **1997**, *6*, 226−233.
(47) Chabal, Y. J.; Higashi, G. S.; Raghavachari, K.; Burrows, V. A. Infrared Spectroscopy of Si(111) and Si(100) Surfaces after HF Treatment: Hydrogen Termination and Surface Morphology. *J. Vac. Sci. Technol., A* **1989**, *7*, 2104−2109.
(48) Takahagi, T.; Nagai, I.; Ishitani, A.; Kuroda, H.; Nagasawa, Y. The Formation of Hydrogen Passivated Silicon Single-Crystal Surfaces Using Ultraviolet Cleaning and HF Etching. *J. Appl. Phys.* **1988**, *64*, 3516−3521.
(49) Tyagi, V.; Gupta, A. K. Novel and Convenient Ozonating Approach to cis-Hydroxylation of Cyclic Vinylsilanes. *Synth. Commun.* **2013**, *43*, 1915−1919.
(50) Gleason-Rohrer, D. C.; Brunschwig, B. S.; Lewis, N. S. Measurement of the Band Bending and Surface Dipole at Chemically Functionalized Si(111)/Vacuum Interfaces. *J. Phys. Chem. C* **2013**, *117*, 18031−18042.
(51) Ristein, J. Surface Transfer Doping of Semiconductors. *Science* **2006**, *313*, 1057−1058.
(52) Landstrass, M. I.; Ravi, K. V. Hydrogen Passivation of Electrically Active Defects in Diamond. *Appl. Phys. Lett.* **1989**, *55*, 1391−1393.
(53) Gi, R. S.; Mizumasa, T.; Akiba, Y.; Hirose, Y.; Kurosu, T.; Iida, M. Formation Mechanism of p-Type Surface Conductive Layer on Deposited Diamond Films. *Jpn. J. Appl. Phys.* **1995**, *34*, 5550−5555.
(54) Maier, F.; Riedel, M.; Mantel, B.; Ristein, J.; Ley, L. Origin of Surface Conductivity in Diamond. *Phys. Rev. Lett.* **2000**, *85*, 3472−3475.
(55) Kong, J.; Franklin, N. R.; Zhou, C.; Chapline, M. G.; Peng, S.; Cho, K.; Dai, H. Nanotube Molecular Wires as Chemical Sensors. *Science* **2000**, *287*, 622−625.
(56) Collins, P. G.; Bradley, K.; Ishigami, M.; Zettl, A. Extreme Oxygen Sensitivity of Electronic Properties of Carbon Nanotubes. *Science* **2000**, *287*, 1801−1804.
(57) Strobel, P.; Riedel, M.; Ristein, J.; Ley, L. Surface Transfer Doping of Diamond. *Nature* **2004**, *430*, 439−441.
(58) Qi, D.; Chen, W.; Gao, X.; Wang, L.; Chen, S.; Loh, K. P.; Wee, A. T. S. Surface Transfer Doping of Diamond (100) by Tetrafluorotetracyanoquinodimethane. *J. Am. Chem. Soc.* **2007**, *129*, 8084−8085.
(59) Rietwyk, K. J.; Smets, Y.; Bashouti, M.; Christiansen, S. H.; Schenk, A.; Tadich, A.; Edmonds, M. T.; Ristein, J.; Ley, L.; Pakes, C. I. Charge Transfer Doping of Silicon. *Phys. Rev. Lett.* **2014**, *112*, 155502.
(60) Tordjman, M.; Saguy, C.; Bolker, A.; Kalish, R. Superior Surface Transfer Doping of Diamond with MoO_3. *Adv. Mater. Interfaces* **2014**, *1*, 1300155.
(61) Lambert, J. B.; Zhao, Y.; Emblidge, R. W.; Salvador, L. A.; Liu, X.; So, J.-H.; Chelius, E. C. The β Effect of Silicon and Related Manifestations of σ Conjugation. *Acc. Chem. Res.* **1999**, *32*, 183−190.

DOI: 10.1021/acsami.6b03326
ACS Appl. Mater. Interfaces 2016, 8, 13157−13165

(62) Maliakal, A. J.; Chen, J. Y.-C.; So, W.-Y.; Jockusch, S.; Kim, B.; Ottaviani, M. F.; Modelli, A.; Turro, N. J.; Nuckolls, C.; Ramirez, A. P. Mechanism for Oxygen-Enhanced Photoconductivity in Rubrene: Electron Transfer Doping. *Chem. Mater.* **2009**, *21*, 5519−5526.
(63) Peterson, D. J. α-Neutral Heteroatom-Substituted Organometallic Compounds. *Organomet. Chem. Rev. A* **1972**, *7*, 295−358.
(64) Chuang, T. J. Electron Spectroscopy Study of Silicon Surfaces Exposed to XeF_2 and the Chemisorption of SiF_4 on Silicon. *J. Appl. Phys.* **1980**, *51*, 2614−2619.
(65) Cypryk, M. Hydrolysis of Fluorosilanes: A Theoretical Study. *J. Phys. Chem. A* **2005**, *109*, 12020−12026.
(66) Höhne, A.; Yu, L.; Mu, L.; Reiher, M.; Voigtmann, U.; Klar, U.; Graham, K.; Schubiger, P. A.; Ametamey, S. M. Organofluorosilanes as Model Compounds for ^{18}F-Labeled Silicon-Based PET Tracers and their Hydrolytic Stability: Experimental Data and Theoretical Calculations. *Chem. - Eur. J.* **2009**, *15*, 3736−3743.
(67) Michalak, D. J.; Amy, S. R.; Aureau, D.; Dai, M.; Estève, A.; Chabal, Y. J. Nanopatterning Si(111) surfaces as a selective surface-chemistry route. *Nat. Mater.* **2010**, *9*, 266−271.
(68) Gräf, D.; Grundner, M.; Schulz, R. Reaction of Water with Hydrofluoric Acid Treated Silicon(111) and (100) Surfaces. *J. Vac. Sci. Technol., A* **1989**, *7*, 808−813.
(69) Cerofolini, G. F.; Mascolo, D.; Vlad, M. O. A Model for Oxidation Kinetics in Air at Room Temperature of Hydrogenterminated (100) Si. *J. Appl. Phys.* **2006**, *100*, 054308.
(70) Yerushalmi, Z. F.; Ho, J. C.; Fan, Z.; Javey, A. Phosphine Oxide Monolayers on SiO_2 Surfaces. *Angew. Chem., Int. Ed.* **2008**, *47*, 4440−4442.
(71) Shay, R. H.; Diel, B. N.; Schubert, D. M.; Norman, A. D. Synthesis and Borane Coordination of Primary Alkenyl- and Alkynylphosphines. *Inorg. Chem.* **1988**, *27*, 2378−2382.
(72) Loscutoff, P. W.; Bent, S. F. Reactivity Of The Germanium Surface: Chemical Passivation and Functionalization. *Annu. Rev. Phys. Chem.* **2006**, *57*, 467−495.
(73) Rosso, M.; Giesbers, M.; Arafat, A.; Schroën, K.; Zuilhof, H. Covalently Attached Organic Monolayers on SiC and Si_xN_4 Surfaces: Formation Using UV Light at Room Temperature. *Langmuir* **2009**, *25*, 2172−2180.
(74) Strother, T.; Knickerbocker, T.; Russell, J. N.; Butler, J. E.; Smith, L. M.; Hamers, R. J. Photochemical Functionalization of Diamond Films. *Langmuir* **2002**, *18*, 968−971.

DOI: 10.1021/acsami.6b03326
ACS Appl. Mater. Interfaces 2016, 8, 13157−13165